

Fractional nonlinear electrical lattice

Mario I. Molina 

Departamento de Física, Facultad de Ciencias, Universidad de Chile, Casilla 653, Santiago, Chile



(Received 2 June 2021; accepted 10 August 2021; published 24 August 2021)

We examine the linear and nonlinear modes of a one-dimensional nonlinear electrical lattice, where the usual discrete Laplacian is replaced by a fractional discrete Laplacian. This induces a long-range intersite coupling that, at long distances, decreases as a power law. In the linear regime, we compute both the spectrum of plane waves and the mean-square displacement (MSD) of an initially localized excitation, in closed form in terms of regularized hypergeometric functions and the fractional exponent. The MSD shows ballistic behavior at long times, $\text{MSD} \sim t^2$ for all fractional exponents. When the fractional exponent is decreased from its standard integer value, the bandwidth decreases and the density of states shows a tendency towards degeneracy. In the limit of a vanishing exponent, the system becomes completely degenerate. For the nonlinear regime, we compute numerically the low-lying nonlinear modes, as a function of the fractional exponent. A modulational stability computation shows that, as the fractional exponent decreases, the number of electrical discrete solitons generated also decreases, eventually collapsing into a single soliton.

DOI: [10.1103/PhysRevE.104.024219](https://doi.org/10.1103/PhysRevE.104.024219)

I. INTRODUCTION

It has been quite a long time since the earlier correspondence between Leibnitz and L'Hopital took place, concerning possible generalizations of the concept of a derivative and whether it made sense to ask questions such as what is the half derivative of a function. The basic starting point was the calculation of $d^\alpha x^k/dx^\alpha$, where α is a noninteger number. This means

$$\frac{d^n x^k}{dx^n} = \frac{\Gamma(k+1)}{\Gamma(k-n+1)} x^{k-n} \rightarrow \frac{d^\alpha x^k}{dx^\alpha} = \frac{\Gamma(k+1)}{\Gamma(k-\alpha+1)} x^{k-\alpha}. \quad (1)$$

From Eq. (1) the fractional derivative of an analytic function $f(x) = \sum_k a_k x^k$ can be computed by deriving term by term. However, this basic procedure is not exempt from ambiguities. For instance, $(d^\alpha/dx^\alpha)1 = (d^\alpha x^0/dx^\alpha) = [1/\Gamma(1-\alpha)]x^{-\alpha} \neq 0$, according to Eq. (1). However, one could have also taken $(d^{\alpha-1}/dx^{\alpha-1})(d/dx)1 = 0$. The initial studies were followed later by rigorous work by several people including Euler, Laplace, Riemann, and Caputo, to name some, and promoted fractional calculus from a mathematical curiosity to a full-blown research field [1–4]. Several possible definitions for the fractional derivative have been obtained, each one with its own advantages and disadvantages. One of the most used definitions is the Riemann-Liouville form

$$\left(\frac{d^\alpha}{dx^\alpha}\right)f(x) = \frac{1}{\Gamma(1-\alpha)} \frac{d}{dx} \int_0^x \frac{f(s)}{(x-s)^\alpha} ds, \quad (2)$$

and another common form is the Caputo formula,

$$\left(\frac{d^\alpha}{dx^\alpha}\right)f(x) = \frac{1}{\Gamma(1-\alpha)} \int_0^x \frac{f'(s)}{(x-s)^\alpha} ds, \quad (3)$$

where $0 < \alpha < 1$. This formalism that extends the usual integer calculus to a fractional one, with its definitions of a fractional integral and fractional derivative, has found application in several fields: fluid mechanics [5], fractional kinetics and anomalous diffusion [6–8], strange kinetics [9], fractional quantum mechanics [10,11], Levy processes in quantum mechanics [12], plasmas [13], electrical propagation in cardiac tissue [14], biological invasions [15], and epidemics [16].

On the other hand, one of the most interesting concepts in nonlinear physics is that of a soliton. It is a solitary wave solution of certain nonlinear differential equations and is characterized by having a spatial profile that remains undeformed upon time evolution. The origin of this behavior lies in a balance between dispersion and nonlinearity. Initially found as solutions of some system of coupled anharmonic oscillators, continuous and discrete solitons have by now been predicted and observed in a wide variety of settings: fluids [17–19], biology (low-frequency collective motion in proteins) [20], optics [21–23], magnetism [24,25], and nuclear physics [26]. In particular, discrete solitons have also been predicted and observed in nonlinear electrical transmission lines [27–34]. The reason is that a nonlinear electrical network can be regarded as a set of coupled anharmonic oscillators.

In this paper, we aim at examining the consequences of the use of a fractional discrete Laplacian on the existence and stability of discrete soliton modes, as well as on the transport of excitations in an electrical bi-inductive electrical network (Fig. 1). As we will see, fractionality changes the spectrum of plane waves, with a bandwidth that decreases with decreasing α and a density of states which also decreases its width, becoming completely degenerate when $\alpha \rightarrow 0$. Interestingly, the mean-square displacement of an initially localized excitation is always ballistic at long times, independently of the value of the fractional exponent, but the number of discrete solitons

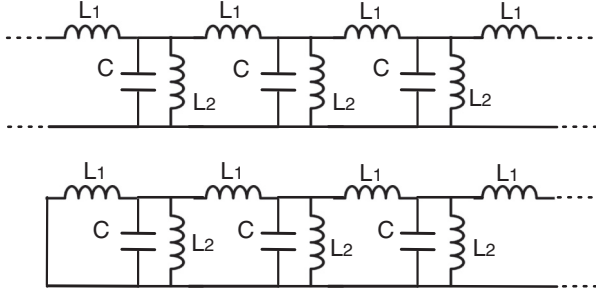


FIG. 1. Infinite (top) and semi-infinite (bottom) bi-inductive electrical lattice (after Ref. [34]).

generated by the modulational stability mechanism depends strongly on the value of the fractional exponent.

II. MODEL

Figure 1 shows a bi-inductive electrical lattice composed of a one-dimensional array of LC circuits coupled inductively. L_1 and L_2 are the inductances and C_n is the nonlinear capacitance of the n th unit, given by $C_n = C_0(1 + \chi_1 + \chi_3 U_n^2)$, where C_0 is the capacitance in vacuum, χ_1 is the linear susceptibility, χ_3 is the third-order susceptibility, and U_n is the voltage drop across the n th capacitor. The nonlinear capacitance C_n can be obtained by inserting a Kerr dielectric material between the capacitor plates. The electrical charge Q_n on the n th capacitor is given by $Q_n = C_n U_n$. After using Kirchhoff's law, the equations for the voltages are

$$\frac{d^2 Q_n}{dt^2} = \frac{1}{L_1}(U_{n+1} - 2U_n + U_{n-1}) - \frac{1}{L_2}U_n. \quad (4)$$

After inserting the expression for Q_n in terms of U_n and after introducing dimensionless variables, we obtain

$$\frac{d^2}{d\tau^2} \{(1 + \chi_1)V_n + \gamma V_n^3\} = (V_{n+1} - 2V_n + V_{n-1}) - \omega^2 V_n, \quad (5)$$

where $V_n = U_n/U_c$, $\gamma = \chi_3 U_c^2$, $\omega^2 = (\omega_2/\omega_1)^2$, $\tau = \omega_1 t$, where $\omega_1 = 1/\sqrt{L_1 C_0}$ and $\omega_2 = 1/\sqrt{L_2 C_0}$ are the resonant frequencies and U_c is a characteristic voltage.

The first term on the right-hand side of Eq. (5) is the discrete Laplacian $\Delta_n V_n = V_{n+1} - 2V_n + V_{n-1}$. Thus, we can write

$$\frac{d^2}{d\tau^2} \{(1 + \chi_1)V_n + \gamma V_n^3\} - \Delta_n V_n + \omega^2 V_n = 0. \quad (6)$$

We now promote this discrete one-dimensional Laplacian to its fractional form, by using results by Roncal *et al.* [35] in which an expression is obtained for the α th power of the discrete Laplacian,

$$(-\Delta_n^\alpha)V_n = \sum_{m \neq n} K^\alpha(n-m)(V_n - V_m), \quad (7)$$

where

$$K^\alpha(m) = L_\alpha \frac{\Gamma(|m| - \alpha)}{\Gamma(|m| + 1 + \alpha)}, \quad (8)$$

with

$$L_\alpha = \frac{4^\alpha \Gamma(\alpha + (1/2))}{\sqrt{\pi} |\Gamma(-\alpha)|}, \quad (9)$$

and $0 < \alpha < 1$ is the fractional exponent.

Thus, the main equation reads

$$\frac{d^2}{d\tau^2} \{(1 + \chi_1)V_n + \gamma V_n^3\} + \sum_{m \neq n} K^\alpha(n-m)(V_n - V_m) + \omega^2 V_n = 0. \quad (10)$$

As we can see, the immediate effect of a fractional discrete Laplacian is to introduce nonlocal interactions via a symmetric kernel $K^\alpha(n-m)$. Using the relation $\Gamma(n+\alpha) = \Gamma(n)\alpha^n$, we obtain the asymptotic expression

$$K^\alpha(m) = 1/|m|^{1+2\alpha} \quad (|m| \rightarrow \infty), \quad (11)$$

i.e., a power-law decrease of the coupling with distance. This is interesting since in most tight-binding treatments in molecular systems and in optics, the coupling between units decreases exponentially. In fact, while for $\alpha = 1$, the non-fractional case, the coupling behaves as $1/|m|^3$ as is proper for a dipole-dipole interaction between the inductors, as α decreases, the coupling range increases, and in the limit of small α , the coupling goes as $1/|m|$, the longest of them all.

III. STATIONARY MODES

Let us look for the stationary modes, in the form $V_n(t) = V_n \cos(\Omega\tau + \phi)$. In order to keep things simple, we use the rotating-wave approximation (RWA), where in $\cos(\Omega\tau + \phi)^3$ we neglect the higher harmonic: $V_n(t)^3 = V_n^3 \cos(\Omega\tau + \phi)^3 \approx (3/4)V_n^3 \cos(\Omega\tau + \phi)$. The stationary equation becomes

$$-\Omega^2 \{(1 + \chi_1)V_n + (3/4)\gamma V_n^3\} + \sum_{m \neq n} K^\alpha(n-m)(V_n - V_m) + \omega^2 V_n = 0. \quad (12)$$

Let us consider first the linear case ($\gamma = 0$),

$$\Omega^2 \{(1 + \chi_1)V_n\} = \omega^2 V_n + \sum_{m \neq n} K^\alpha(n-m)(V_n - V_m), \quad (13)$$

and look for the dispersion relation of plane waves, $V_n = A e^{ikn}$. One obtains

$$\Omega^2(1 + \chi_1) = \omega^2 + 4 \sum_{q \neq 0} K_q^\alpha \sin^2(qk/2). \quad (14)$$

This expression can be recast in closed form as

$$(1 + \chi_1)\Omega^2 = \omega^2 + 2 \frac{\Gamma(2\alpha)}{\Gamma(1 + \alpha)\Gamma(\alpha)} \times [1 - \alpha(e^{-ik} {}_2F_1(1, 1 - \alpha, \alpha + 2; e^{-ik}) + e^{ik} {}_2F_1(1, 1 - \alpha, \alpha + 2; e^{ik}))], \quad (15)$$

where the ${}_2F_1$ are the regularized hypergeometric functions. Figure 2 shows the dispersion $\Omega^2(k)$ for several fractional exponents α . At $\alpha = 1$, the standard case, the band is contained between $\omega^2/(1 + \chi_1)$ and $(\omega^2 + 4)/(1 + \chi_1)$. As α is decreased towards 0, the bandwidth decreases steadily, and at $\alpha \rightarrow 0^+$, the band becomes contained between $\omega^2/(1 + \chi_1)$

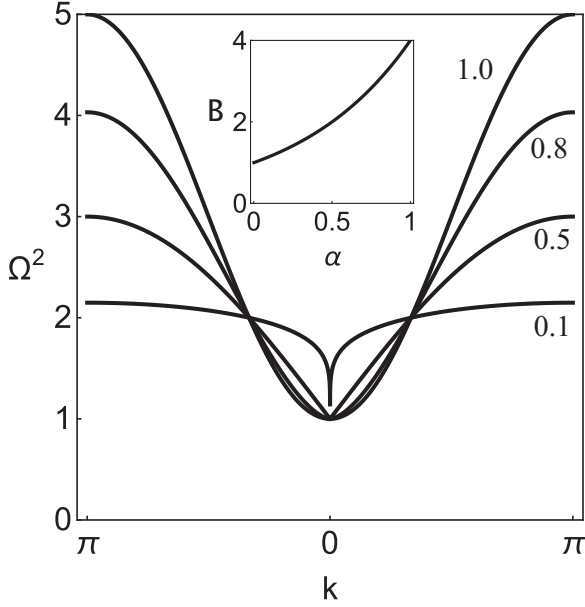


FIG. 2. Dispersion relation for several fractional exponents, for $\chi_1 = 0$ and $\omega^2 = 1$. The number on each curve denotes the value of the fractional exponent α . Inset: Bandwidth Δ as a function of fractional exponent, α .

and $(1 + \omega^2)/(1 + \chi_1)$. The bandwidth, defined by $B(\alpha) = \Omega^2(\alpha, \pi) - \Omega^2(\alpha, 0)$, is given in closed form by

$$B(\alpha) = \frac{4\alpha\Gamma(1 - \alpha)\Gamma(\alpha)}{\pi(1 + \chi_1)} \sin(\alpha\pi) [{}_2F_1(1, 1 - \alpha, 2 + \alpha, -1) + {}_2F_1(1, 1 - \alpha, 2 + \alpha, 1)],$$

and is shown in the inset of Fig. 2.

Figure 3 shows the spatial profiles of all eigenmodes for several fractional exponents. This plot is obtained after stacking the mode profiles one after the other, according to their eigenvalues. Clearly, as α decreases the eigenvalues become more and more confined to an ever-decreasing energy range. In the limit $\alpha \rightarrow 0$, all the eigenvalues become confined to the band $\omega^2/(1 + \chi_1) < \Omega^2 < (1 + \omega^2)/(1 + \chi_1)$. On the other hand, Fig. 4 shows the density of states (DOS)

$$D(\Omega^2) = (1/N) \sum_m \delta(\Omega^2 - \Omega_m^2), \quad (16)$$

where N is the number of sites and the sum is over all modes. We notice that, for all fractional exponents, the DOS displays expected van Hove singularities, of finite height due to the finite-size effects. As the fractional exponent decreases from the standard case ($\alpha = 1$), the DOS high-energy boundary starts receding towards the low-energy boundary, which stays always in place during the process. Due to normalization, this narrowing process also increases the height of the DOS. In the limit of $\alpha \rightarrow 0$, the DOS diverges at $\Omega^2 = (1 + \omega^2)/(1 + \chi_1)$, and the system becomes completely degenerate.

Let us now look at the mean-square displacement (MSD) that serves to monitor the propagation of electrical excitations. The MSD is defined as

$$\langle n^2 \rangle = \sum_n n^2 |V_n(\tau)|^2 / \sum_n |V_n(\tau)|^2. \quad (17)$$

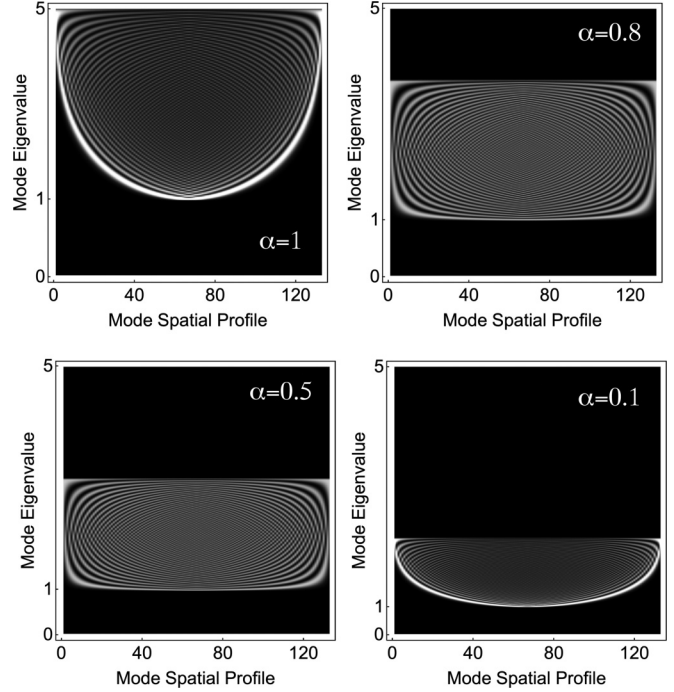


FIG. 3. Density plot of the spatial profiles $|V_n|^2$ of the linear modes ordered according to their eigenvalue ($N = 133$, $\omega = 1$, $\chi_1 = 1$).

For a completely localized initial voltage $V_n(0) = A \delta_{n0}$ and no currents, $(dV_n/d\tau)(0) = 0$, we have formally

$$V_n(\tau) = (A/4\pi) \int_{-\pi}^{\pi} e^{i(kn - \Omega_k)\tau} dk + (A/4\pi) \int_{-\pi}^{\pi} e^{i(kn + \Omega_k)\tau} dk,$$

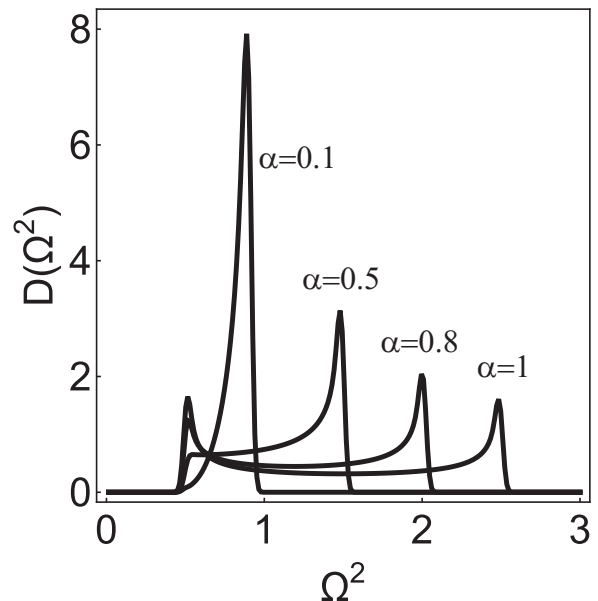


FIG. 4. Density of states vs mode frequency for several fractional exponents. ($w = 1$, $\chi_1 = 1$, $N = 133$.)

where Ω_k is given by Eq. (15). After replacing this form for $V_n(\tau)$ into Eq. (17), one obtains after some algebra, a closed-form expression for $\langle n^2 \rangle$:

$$\langle n^2 \rangle = \frac{(1/2\pi) \int_{-\pi}^{\pi} dk (d\Omega_k/dk)^2 [1 - \cos(2\Omega_k \tau)] \tau^2}{1 + (1/2\pi) \int_{-\pi}^{\pi} dk \cos(2\Omega_k \tau)}. \quad (18)$$

As we can see from the structure of Eq. (18), as time τ increases, the contributions from the cosine terms to the integrals decrease and, at long times, $\langle n^2 \rangle$ approaches a ballistic behavior,

$$\langle n^2 \rangle = \left[\frac{1}{2\pi} \int_{-\pi}^{\pi} \left(\frac{d\Omega(k)}{dk} \right)^2 dk \right] \tau^2 \quad (\tau \rightarrow \infty), \quad (19)$$

while at short times,

$$\langle n^2 \rangle = \left[\frac{1}{2\pi} \int_{-\pi}^{\pi} \left(\Omega_k \frac{d\Omega_k}{dk} \right)^2 dk \right] \tau^4 \quad (t \rightarrow 0). \quad (20)$$

Since the transport exponent is defined as the one corresponding to the dominant behavior at long times, we conclude that the asymptotic transport of our system is ballistic, $\langle n^2 \rangle \sim g(\alpha)\tau^2$, where we can identify $\sqrt{g(\alpha)}$ as a kind of characteristic “speed” for the ballistic propagation. This speed depends implicitly on the fractional exponent through Ω_k^2 , but the ballistic exponent is valid for all $0 < \alpha < 1$.

IV. NONLINEAR ELECTRICAL MODES

We now turn our attention to the nonlinear modes of the system, which are solutions to Eq. (12), with $\gamma \neq 0$. These equations constitute a system of nonlinear coupled difference equations, of the form $\vec{F}(\vec{V}) = 0$, where $\vec{V} = (V_1, V_2, \dots, V_N)$. Numerical solutions are obtained by using a multidimensional Newton-Raphson scheme. This method solves the system of nonlinear equations starting from a seed, which is supposed to be an approximate solution. If the initial guess is close to the real solution, convergence to the solution will be quickly reached. For instance, to find the fundamental solution in the bulk which has a single localized maximum, we use as a guess something like $(0, \dots, 0, A, 0, \dots, 0)$. For the fundamental surface mode, we would use $(A, 0, \dots, 0, 0)$. Figure 5 shows examples of some bulk and surface modes obtained from this procedure. These discrete soliton modes lie outside the linear band (shaded areas in Fig. 7). For a given exponent α , the spatial profiles of all these modes are qualitatively similar to the ones found for the standard integer case ($\alpha = 1$).

In addition to these localized modes, there are also nonlinear extended modes such as a uniform profile i.e., a flat front $V_n(t) = A \cos(\Omega t)$. Let us compute the dynamical evolution of this uniform state and see whether the profile keeps its form in time. When it does not, we have an instability known as a modulation instability (MI) [36,37]. As a concrete example, let us compute the MI for our electrical system. We use an array of $N = 104$ units, a maximum evolution time of $\tau_{\max} = 500$, an initial amplitude of $A = 1$, $\chi_1 = 0$, and a nonlinear susceptibility of $\chi_3 = 1$. The fractional exponent chosen is $\alpha = 0.1$, a value substantially away from the standard case ($\alpha = 1$). At both extremes of the array, we perturb the amplitudes as $A_1 \rightarrow 1.01A_1$, $A_N \rightarrow 1.01A_N$. Results from

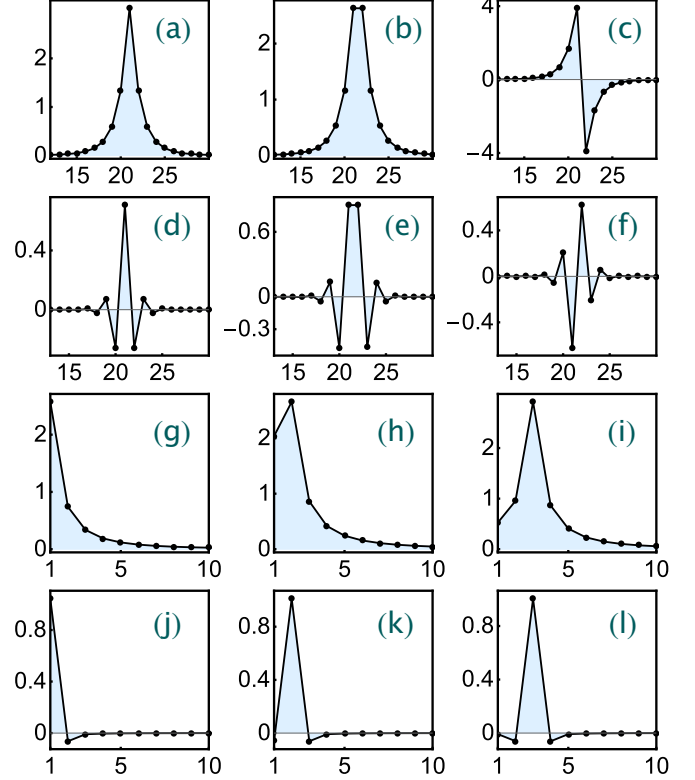


FIG. 5. Examples of some low-lying nonlinear modes of the electrical lattice for $\chi_1 = 0$ and fractional exponent $\alpha = 0.5$. On each plot, the vertical axis denotes the mode amplitude, while the horizontal axis indicate positions along the electrical array. First row: Bulk modes for $\chi_3 = 1$ (focusing nonlinearity). (a)–(c) denote the odd, even, and twisted modes, respectively. Second row: Bulk modes for $\chi_3 = -1$ (defocusing nonlinearity). (d)–(f) denote the odd, even, and twisted modes, respectively. Third row: Surface modes for $\chi_3 = 1$. (g)–(i) denote the first-, second-, and third-layer modes, respectively. Fourth row: Surface modes for $\chi_3 = -1$. (j)–(l) denote the first-, second-, and third-layer modes, respectively.

this procedure are shown in Fig. 6, where we show density plots where the height represents the amplitude of the voltage, while the vertical and horizontal axes denote the time and the position along the array, respectively. Each plot corresponds to a different fractional exponent. In all cases we observe the presence of modulational instability where the uniform front collapses after some time into a number of filament-like structures that persist in time, that can be interpreted as discrete solitons. Indeed, previous works on the discrete nonlinear Schrödinger (DNLS) equation have identified MI as a mechanism for the creation of discrete solitons. The same phenomenon seems to be at work here. We observe that as the fractional exponent decreases, the number of discrete solitons created decreases. At small α , only one filament remains. The solitons generated are more or less equidistant from each other and no merging of them is observed for the times explored.

Let us now examine the linear stability of the two lowest-lying stationary modes shown in Figs. 5(a) and 5(d), that is, the modes with the lowest power content. Let us focus on the electric charge on the capacitor, rather than the voltage across it. Using the relation $Q_n = C_n U_n$, with

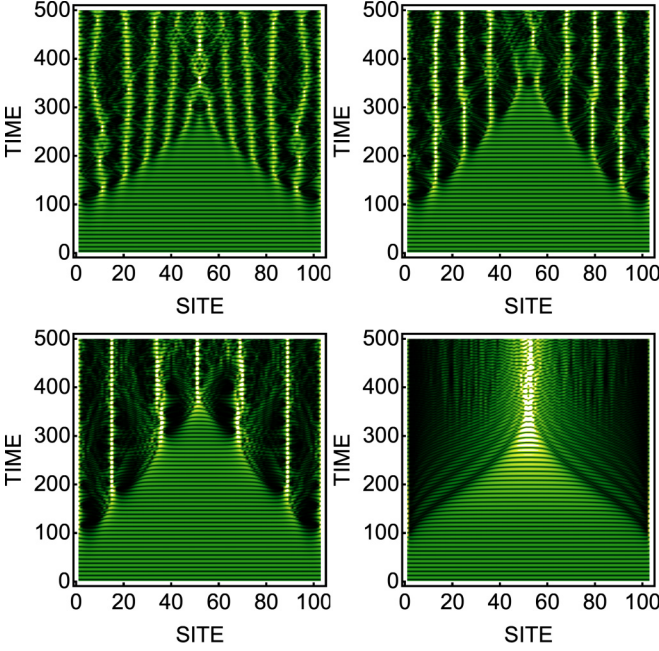


FIG. 6. An example of modulational stability for the electrical array, for several fractional exponent values. Top left: $\alpha = 1$. Top right: $\alpha = 0.7$. Bottom left: $\alpha = 0.5$. Bottom right: $\alpha = 0.1$. In all cases $\chi_1 = 0$, $\chi_3 = 1$.

$C_n = C_0(1 + \chi_3 U_n^2)$ (i.e., $\chi_1 = 0$), one has approximately $U_n \approx (Q_n/C_0)[1 - (\chi_3/C_0^2)Q_n^2]$. This assumes a small nonlinear contribution. After replacing this into Eq. (10) and using dimensionless variables, we obtain

$$\frac{d^2 q_n}{d\tau^2} + \sum_{m \neq n} K^\alpha(n-m)(q_n - q_m) + \gamma(q_{n+1}^3 - 2q_n^3 + q_{n-1}^3) + \omega^2 q_n(\gamma - \omega q_n) = 0. \quad (21)$$

For a stationary mode $q_n(\tau) = q_n \cos(\Omega\tau)$, we obtain

$$-\Omega^2 q_n + \sum_{m \neq n} K^\alpha(n-m)(q_n - q_m) + (3/4)\gamma(q_{n+1}^3 - 2q_n^3 + q_{n-1}^3) + \omega^2 q_n(\gamma - \omega q_n) = 0, \quad (22)$$

where we have employed the rotating-wave approximation. The linear stability analysis proceeds as usual by perturbing the mode as $q_n(\tau) \rightarrow q_n \cos(\Omega\tau) + \Delta_n$ with $|\Delta_n| \ll |q_n|$. After replacing this form into Eq. (21), and after keeping only the linear terms on Δ_n , one obtains a linear differential equation for Δ_n ,

$$\frac{d^2}{d\tau^2} \Delta_n + \left\{ \sum_{m \neq n} K^\alpha(n-m) - (9/4)\gamma q_n^2(1 - \omega^2) \right\} \Delta_n - \sum_{m \neq n} K^\alpha(n-m)\Delta_m + (9/4)\gamma(q_{n+1}^2 \Delta_{n+1} + q_{n-1}^2 \Delta_{n-1}), \quad (23)$$

which can be cast as a matrix equation

$$(d^2/d\tau^2)\vec{\Delta} + \mathbf{A}\vec{\Delta} = 0, \quad (24)$$

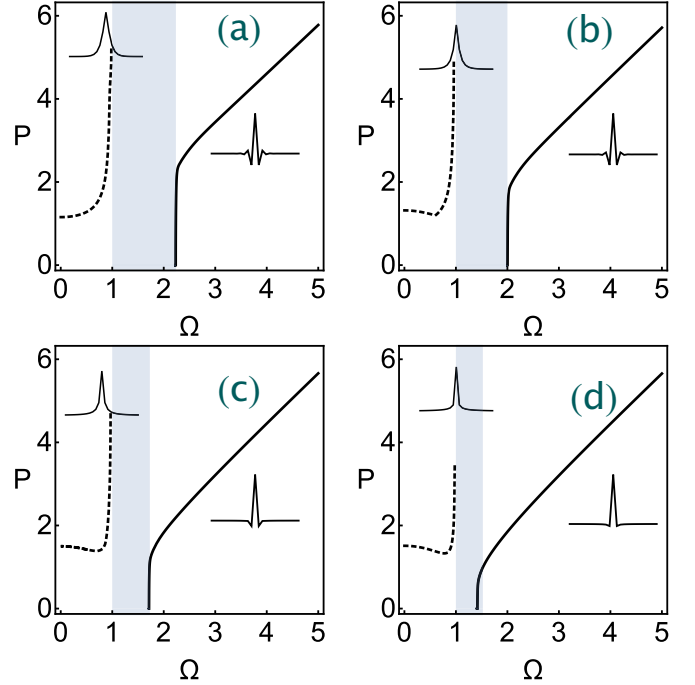


FIG. 7. Bifurcation plot for the two lowest-lying nonlinear modes. The power content P of the modes is plotted as a function of the frequency Ω , for several fractional exponents: (a) $\alpha = 0.9999$, (b) $\alpha = 0.8$, (c) $\alpha = 0.5$, and (d) $\alpha = 0.2$. Solid (dashed) curves denote stability (instability). The typical shape of the mode profiles is also sketched.

where $\vec{\Delta} = (\Delta_1, \Delta_2, \dots, \Delta_N)$. Thus, stability will occur if all the eigenvalues of matrix \mathbf{A} are positive, and instability when there is at least a single negative eigenvalue. The bifurcation diagram is usually displayed as the power content versus the frequency. Figure 7 shows this power $P = \sum_n |q_n|^2$ versus the frequency of the mode Ω for the two lowest-lying modes, one for $\chi_3 > 0$ (focusing nonlinearity) and the other for $\chi_3 < 0$ (defocusing nonlinearity). This is computed for several fractional exponents α . An empirical check for the stability of the fundamental soliton is the Vakhitov-Kolokolov criterion [38–40]: If $dP/d\Omega > 0$, the fundamental mode is stable, otherwise, if $dP/d\Omega < 0$, the fundamental mode is unstable. This is obeyed in our case, as Fig. 7 shows.

V. CONCLUSIONS

We have examined the effect of using a fractional definition of the Laplacian for a one-dimensional array of coupled nonlinear electrical units. The introduction of fractionality gives rise to a nonlocal coupling between the units, which at long distances decreases as a power law.

In the linear regime, and in the presence of fractionality, there are modes in the form of electric plane waves whose dispersion relation was computed in closed form in terms of hypergeometric functions. The main effect of a fractional exponent is the reduction of the bandwidth with decreasing exponent. The density of states shows that, as the exponent decreases, the states shift to the lower band edge. In the limit of a vanishing fractional exponent, all the states become

completely degenerate, at an energy value proportional to the ratio of the fundamental resonant frequencies of the array. The mean-square displacement of an initially localized electric excitation was calculated in closed form, showing a ballistic behavior at long times, while at short times the behavior was quartic in time.

In the nonlinear regime, the nonlinear electric modes were computed with the help of the rotating-wave approximation. The bulk and surface profiles were similar to their standard, not fractional, counterpart. The modulational stability of the array was also computed. As expected, the onset of instability gave rise to a number of localized spatial structures that persisted in time, such as discrete solitons, similar to what is observed in the standard case. These electric solitons form a sort of miniarray and its number depended strongly upon the value of the fractional exponent, decreasing their number as the exponent decreases. Finally, we computed the linear stability of the two lowest-lying nonlinear modes. While in the semi-infinite gap the fundamental mode is stable, inside the finite gap, the mode turned out to be unstable.

Even though it might seem that the fractional effects could hardly be observed using macroscopic electric circuitry, we conjecture that these effects could be observed at the nanoscale, with the use of nanoscopic circuits [41,42] that have proven promising for the creation and manipulation of novel metamaterials. It must not be forgotten that induction coupling decreases slowly in space, at least as $1/|\mathbf{r}|^3$ (for $\alpha = 1$ from dipole-dipole interactions), and even slower for $\alpha < 1$. This behavior is markedly different from the usual coupling in optics and molecular systems where the coupling decreases exponentially with distance. It would then be possible to engineer the distance (i.e., coupling) between the electrical units judiciously to create a fractional transmission line. A possible setup could be an array of mesoscopic split-ring resonators [43] embedded in a dielectric substrate.

ACKNOWLEDGMENT

This work was supported by Fondecyt Grant No. 1200120.

-
- [1] R. Herrmann, *Fractional Calculus—An Introduction for Physicists* (World Scientific, Singapore, 2014).
- [2] B. West, M. Bologna, and P. Grigolini, *Physics of Fractal Operators* (Springer, Berlin, 2003).
- [3] K. S. Miller and B. Ross, *An Introduction to the Fractional Calculus and Fractional Differential Equations* (Wiley, New York, 1993).
- [4] *Applications of Fractional Calculus in Physics*, edited by R. Hilfer (World Scientific, Singapore, 2000).
- [5] L. A. Caffarelli and A. Vasseur, Drift diffusion equations with fractional diffusion and the quasi-geostrophic equation, *Ann. Math.* **171**, 1903 (2010).
- [6] R. Metzler and J. Klafter, The random walk's guide to anomalous diffusion: A fractional dynamics approach, *Phys. Rep.* **339**, 1 (2000).
- [7] I. M. Sokolov, J. Klafter, and A. Blumen, Fractional kinetics, *Phys. Today* **55** (11), 48 (2002).
- [8] G. M. Zaslavsky, Chaos, fractional kinetics, and anomalous transport, *Phys. Rep.* **371**, 461 (2002).
- [9] M. F. Shlesinger, G. M. Zaslavsky, and J. Klafter, Strange kinetics, *Nature (London)* **363**, 31 (1993).
- [10] N. Laskin, Fractional quantum mechanics, *Phys. Rev. E* **62**, 3135 (2000).
- [11] N. Laskin, Fractional Schrödinger equation, *Phys. Rev. E* **66**, 056108 (2002).
- [12] N. C. Petroni and M. Pusterla, Levy processes and Schrödinger equation, *Phys. A* **388**, 824 (2009).
- [13] M. Allen, A fractional free boundary problem related to a plasma problem, *Commun. Anal. Geom.* **27**, 1665 (2019).
- [14] A. Bueno-Orovio, D. Kay, V. Grau, B. Rodriguez and K. Burrage, Fractional diffusion models of cardiac electrical propagation: role of structural heterogeneity in dispersion of repolarization, *J. R. Soc., Interface* **11**, 0352 (2014).
- [15] H. Berestycki, J.-M. Roquejoffre, and L. Rossi, The influence of a line with fast diffusion on Fisher-KPP propagation, *J. Math. Biol.* **66**, 743 (2013).
- [16] A. Atangana, Application of fractional calculus to epidemiology, in *Fractional Dynamics*, edited by C. Cattani, H. M. Srivastava, and X.-J. Yang (De Gruyter Open, Warsaw, Poland, 2015).
- [17] *Solitary Waves in Fluids*, edited by R. H. J. Grimshaw (WIT Press, Southampton, UK, 2007).
- [18] G. Michel, F. Bonnefoy, G. Ducrozet, G. Prabhudesai, A. Cazaubiel, F. Copie, A. Tikan, P. Suret, S. Randoux, and E. Falcon, Emergence of Peregrine solitons in integrable turbulence of deep water gravity waves, *Phys. Rev. Fluids* **5**, 082801(R) (2020).
- [19] A. Costa, A. R. Osborne, D. T. Resio, S. Alessio, E. Chrivi, E. Saggese, K. Bellomo, and C. E. Long, Soliton Turbulence in Shallow Water Ocean Surface Waves, *Phys. Rev. Lett.* **113**, 108501 (2014).
- [20] A. S. Davydov, *Solitons in Molecular Systems* (Springer, Dordrecht, 1985).
- [21] F. Abdullaev, S. Darmanyan, and P. Khabibullaev, *Optical Solitons* (Springer, Berlin, 1993).
- [22] A. Hasegawa and M. Matsumoto, *Optical Solitons in Fibers* (Springer, Berlin, 2003).
- [23] Y. S. Kivshar and G. P. Agrawal, *Optical Solitons: From Fibers to Photonic Crystals* (Academic, Cambridge, MA, 2003).
- [24] A. M. Kosevich, B. A. Ivanov, and A. S. Kovalev, Magnetic solitons, *Phys. Rep.* **194**, 117 (1990).
- [25] N. V. Ostrovskaya, Magnetic solitons, in *Soliton-Driven Photonics*, edited by A. D. Boardman and A. P. Sukhorukov (Springer, Dordrecht, 2001).
- [26] E. F. Hefter, Solitons in nuclear physics - a review, in *Condensed Matter Theories*, edited by J. S. Arponen, R. F. Bishop, and M. Manninen (Springer, Boston, 1988).
- [27] R. Hirota and K. Suzuki, Studies on lattice solitons by using electrical networks, *J. Phys. Soc. Jpn.* **28**, 1366 (1970).
- [28] T. Kuusela, J. Hietarinta, and B. A. Malomed, Numerical study of solitons in the damped ac-driven Toda lattice, *J. Phys. A: Math. Gen.* **26**, L21 (1993).

- [29] D. Yemele, P. Marquie, and J. M. Bilbault, Long-time dynamics of modulated waves in a nonlinear discrete LC transmission line, *Phys. Rev. E* **68**, 016605 (2003).
- [30] T. Kuusela, Soliton experiments in a damped ac-driven nonlinear electrical transmission line, *Phys. Lett. A* **167**, 54 (1992).
- [31] R. Stearrett and L. Q. English, Experimental generation of intrinsic localized modes in a discrete electrical transmission line, *J. Phys. D* **40**, 5394 (2007).
- [32] L. Q. English, F. Palmero, J. F. Stormes, J. Cuevas, R. Carretero-Gonzalez, and P. G. Kevrekidis, Nonlinear localized modes in two-dimensional electrical lattices, *Phys. Rev. E* **88**, 022912 (2013).
- [33] F. Palmero, L. Q. English, X.-L. Chen, W. Li, J. Cuevas, and P. G. Kevrekidis, Experimental and numerical observation of dark and bright breathers in the band gap of a diatomic electrical lattice, *Phys. Rev. E* **99**, 032206 (2019).
- [34] M. I. Molina, L. Q. English, M.-H. Chang, and P. G. Kevrekidis, Linear impurity modes in an electrical lattice: Theory and experiment, *Phys. Rev. E* **100**, 062114 (2019).
- [35] O. Ciaurri, L. Roncal, P. R. Stinga, J. L. Torrea, and J. L. Varona, Nonlocal discrete diffusion equations and the fractional discrete Laplacian, regularity and applications, *Adv. Math.* **330**, 688 (2018).
- [36] V. E. Zakharov and L. A. Ostrovsky, Modulation instability: The beginning, *Physica D* **238**, 540 (2009).
- [37] E. Kengne, S. T. Chui, and W. M. Liu, Modulational instability criteria for coupled nonlinear transmission lines with dispersive elements, *Phys. Rev. E* **74**, 036614 (2006).
- [38] N. G. Vakhitov and A. A. Kolokolov, Stationary solutions of the wave equation in a medium with nonlinearity saturation, *Radiophys. Quantum Electron.* **16**, 783 (1973).
- [39] Y. S. Kivshar and G. P. Agrawal, *Optical Solitons: From Fibers to Photonic Crystals* (Academic, Cambridge, MA, 2003).
- [40] N. K. Efremidis, J. Hudock, D. N. Christodoulides, J. W. Fleischer, O. Cohen, and M. Segev, Two-Dimensional Optical Lattice Solitons, *Phys. Rev. Lett.* **91**, 213906 (2003).
- [41] N. Engheta, A. Salandrino, and A. Alu, Circuit Elements at Optical Frequencies: Nanoinductors, Nanocapacitors, and Nanoresistors, *Phys. Rev. Lett.* **95**, 095504 (2005).
- [42] Y. Wang, L. J. Lang, C. H. Lee, B. Zhang, and Y. D. Chong, Topologically enhanced harmonic generation in a nonlinear transmission line metamaterial, *Nat. Commun.* **10**, 1102 (2019).
- [43] F. Martin and R. Marques, Application of split ring resonators to microwave circuit design, in *Applications of Metamaterials*, edited by F. Cappolino (CRC Press, Boca Raton, FL, 2009).